Folding in regions of extension

F. Lévy, C. Jaupart

Geophysical Journal International

Geophys. J. Int. (2011) **185,** 1120–1134 doi: 10.1111/j.1365-246X.2011.05013.x

Folding in regions of extension

F. Lévy* and C. Jaupart

Équipe de Dynamique des Fluides Géologiques, Institut de Physique du Globe de Paris, Sorbonne Paris Cité, Univ. Paris Diderot, UMR 7154 *CNRS,* 1 *rue Jussieu,* 75238 *Paris, France. E-mail: florence.levy@saint-venant-lab.fr*

Accepted 2011 March 7. Received 2011 January 30; in original form 2010 July 7

SUMMARY

Many extension zones have been subjected to folding and shortening in a direction perpendicular to the stretching. Such deformation can be accounted for by the extension of a thin superficial elastic layer overlying a substrate that has small elastic moduli or that deforms in a viscous regime. Laboratory experiments are used to document the wavelength and amplitude of the folds for a range of geometrical configurations. Folding is observed even for very small amounts of extension (less than 1 per cent) with characteristics that are consistent with finite-amplitude scaling laws. Because of the intrinsically 3-D nature of the deformation field, the size of the region affected by folding and the direction of the fold axes depend on the orientation of the extension with respect to the rigid blocks that bound the deforming region. For regions of extension where the elastic thickness is about 10 km, as in the Basin and Range province for example, it is predicted that folding occurs with wavelengths in a 20–40 km range, such that it induces little deformation in the lower crust and maintains a flat Moho discontinuity. These predictions are consistent with the observations. The characteristics of faulting that is associated with such deformation are discussed.

Key words: Continental tectonics: extensional; Folds and folding; Mechanics, theory, and modelling.

1 INTRODUCTION

Folding in regions of extension occurs in a bewildering variety of dimensions and orientations to the direction of extension (Schlische 1995; Janecke *et al.* 1998). Furthermore, folds with different orientations may develop in different domains of the same province (Janecke *et al.* 1998; Faulds *et al.* 2002). At a smaller scale, several types of folds may be observed in a single domain and it is useful to discriminate between them using physical models.

In the following, folding refers to the physical mechanism that generates folds and that is associated with shortening. Thus, in the framework of this paper, folding acts in a direction perpendicular to extension and generates extension-parallel folds, such that their axes are aligned with the extension or lie at a small angle to the extension direction.

Quasi-periodic extension-parallel folds have been documented in many continental extension zones including the Basin and Range province of the Western United States (e.g. Yin 1991; Fletcher & Bartley 1994; Fletcher *et al.* 1995), the central Aegean (Avigad *et al.* 2001; Jolivet *et al.* 2004) and the Norwegian Caledonides (Chauvet & Séranne 1994). The lateral shortening that is associated with such folding is contemporaneous with the extension (Mancktelow & Pavlis 1994; Fletcher & Bartley 1994; Avigad *et al.* 2001). Avigad *et al.* (2001) noted that, in the Aegean, extensional tectonics led to no significant crustal thinning, which indicates that some compensation mechanism has been active. They suggested that this was shortening in a direction perpendicular to the extension. Folding in a direction perpendicular to extension results in metamorphic domes that have been ductilely stretched and that are bounded by normal faults (Mancktelow & Pavlis 1994). The exact mechanism that is responsible for such deformation has been debated for many years. The main question deals with the stress regime that is responsible for extension in one horizontal direction and shortening in the other horizontal direction. Fletcher & Bartley (1994) have argued that a simple uniaxial stress field accounts for the main deformation characteristics, with stretching in the direction of regional extension and constrictional strain in the other horizontal direction. This simple stress field is consistent with earthquake focal mechanisms in the Basin and Range province, for example (Zoback & Zoback 1989). The strain field, in contrast, cannot be reduced to a simple 2-D configuration and must be studied in 3-D. This is shown by the coexistence of extension in one direction and shortening in the other direction as well as fold axes that are slightly oblique to the stretching direction in many instances (Avigad *et al.* 2001). Another important observation is that the Moho discontinuity is flat so that the extension parallel-folds and the associated topography are not isostatically compensated (Tirel *et al.* 2004).

Many analyses have been based on local observations of a few structures. Here, we focus on the large-scale pattern, such that shortening in a direction perpendicular to regional extension proceeds

*Now at: Laboratoire d'Hydraulique Saint-Venant, Joint-Research Unit of CETMEF, EDF R&D and ENPC, 6 Quai Wattier, 78400 Chatou, France.

through folds of nearly identical characteristics with a well-defined spacing. One test of the deformation mechanism is that it accounts for the observed spacing and amplitude of folds. In a pioneering study, Yin (1991) calculated deformation in a thin elastic plate due to applied stresses. He obtained a periodic pattern of domes and basins in only two cases. One involves a periodic variation of the normal stress at the top or base of the plate. In the other case, no vertical load is applied and tension in one horizontal direction and compression in the other horizontal direction are both required for folding. In the analysis of Yin (1991), therefore, no folding can be generated by uniaxial extension, which is at odds with the conclusions of Fletcher & Bartley (1994). This analysis, however, relies on a plate of fixed dimensions, which does not allow for lateral shortening explicitly. A comprehensive study of folding due to compression in 3-D was made by Kaus & Schmalholz (2006) for viscous rheologies. Following Schmalholz *et al.* (2005), these authors emphasized the phenomenon of 'structural softening', such that strain rates in the folded layer are smaller than the background horizontal shortening rate. This applies to other rheologies and stress configurations, including those of this study, and we shall return to this issue in a discussion section. The periodic alternation of basins and ranges has been attributed to necking instabilities by many authors, following Fletcher & Hallet (1983). Theoretical models have been limited to plastic or viscous rheologies for the upper crust, and predict that the spacing between topographic highs and lows is typically two to four times the thickness of the strong upper crustal layer (Ricard & Froidevaux 1986; Zuber *et al.* 1986; Martinod & Davy 1992). Brittle extension of an upper crustal layer has been studied in the laboratory and in numerical calculations (Benes & Davy 1996; Corti 2005; Wijns *et al.* 2005). In this case, extension induces a periodic array of normal faults whose spacing is controlled by the thickness of the brittle layer, but no explicit scaling is available. Most of these models are carried out in two dimensions in a vertical plane and hence cannot account for extension-parallel folds. In all cases, the necking instability induces lateral variations of crustal thickness. Fletcher & Hallet (1983), for example, found that, in their model, the crust beneath the upper plastic layer and the upper mantle is 'characterized by the development of a large structural relief'. This would imply variations of Moho depth, which are not observed beneath regions of extension (Klemperer *et al.* 1986; Gans 1987). Other studies have been focussed on specific aspects of extension regions, such as the flat Moho (Gans 1987) or the distributed regional deformation (Buck 1991). None of these models account for shortening and folding in a direction perpendicular to extension (Mancktelow & Pavlis 1994).

Other than extension-parallel folds, several features of extension regions have not been accounted for by the various models listed earlier. For example, the strike of basins and ranges varies across the Basin and Range province, from a roughly NS direction in the eastern part to a NE–SW in the western part (Eaton 1980) (Fig. 1). Also, there are small, but significant, differences between the directions of extension and fold axes in the Aegean (Avigad *et al.* 2001). These observations attest to the fundamentally 3-D nature of the deformation.

In this study, we argue that some important deformation characteristics of extension zones are acquired in early phases of extension when the amounts of strain are small, such that deformation proceeds in an elastic regime, before the onset of major normal faulting. Marques & Podladchikov (2009) have made the same point for deformation in compression regimes. Specifically, we propose that extension-parallel folds are due to elastic deformation and discuss geometrical controls on the orientation of fold axes. One intrinsic feature of this deformation regime is shortening in a direction perpendicular to extension, which provides a straightforward explanation for the lack of significant crustal thinning that was emphasized by Avigad *et al.* (2001) in the Aegean, for example. The paper is organized as follows. We recapitulate a few observations that demonstrate that folding does occur early during extension and that provide the framework of our study. We then discuss evidence for the important role played by flexural stresses, which are a direct consequence of elastic deformation. We contend that extension-parallel folds are due to a uniaxial extensional stress field and propose that a thin elastic layer controls the initial large-scale deformation pattern. We carry out laboratory experiments that document precisely the characteristics of folding. We rely on theory originally proposed by Cerda *et al.* (2002) and show that the observed wavelength and amplitude of folds are consistent with the theoretical predictions. Simple scaling laws allow easy evaluation of fold characteristics and their dependence on the control variables and physical properties. Because of the 3-D nature of the deformation, we also investigate the influence of the boundary conditions and specifically the influence of the shape and orientation of the rigid domains that bound the extension zone. We show how the intrinsically 3-D nature of elastic deformation can lead to fold axes with different orientations in different parts of the same province. In a discussion section, we evaluate the conditions that are required for fold generation, which include limitations on the elastic plate thickness and on the dimensions of the deforming region. We also discuss the simple model of an elastic sheet in relation to the more complex rheological properties of continental crust and lithospheric mantle. Finally, we study some aspects of the faulting that occurs in association with folding.

2 CHARACTERISTICS OF FOLDING IN REGIONS OF EXTENSION

We briefly recapitulate a few facts about extension and folding, as illustrated by the Aegean and the Basin and Range. In both regions, as shown by the large-scale deformation pattern and small-scale strain analyses, extension develops in an intrinsically 3-D regime involving extension in one direction and shortening in the other.

Extension in the Aegean region started 30 Ma (e.g. Jolivet & Faccenna 2000). Present-day deformation is concentrated in peripheral regions (Dewey 1988; Jolivet & Faccenna 2000). GPS measurements indicate that the current extension direction is North–South (McClusky *et al.* 2000) and has apparently remained relatively constant through time (Jolivet 2001). In the Aegean Sea, extension was accompanied by EW shortening (i.e. perpendicular to the stretching), which started more than 20 Ma (Avigad *et al.* 2001). This shortening resulted in large-scale folded structures which were later exhumed (∼8 Ma) and form the metamorphic domes of Naxos, Paros and Mykonos (Fig. 2). The metamorphic domes have a characteristic spacing in the 20–30 km range, but the Moho discontinuity beneath them shows no associated undulations and is flat (Tirel *et al.* 2004). On a larger scale, the crustal thickness is slightly thicker in the Central Aegean than to the North and South (Jolivet *et al.* 2004). According to Avigad *et al.* (2001), the EW shortening acted to compensate for crustal thinning due to extension, so that the present crustal thickness does not differ significantly from its value prior to extension.

The Basin and Range Province of the western United-States is the largest zone of distributed extension on Earth. It is remarkable for its periodic alternation of topographic highs and lows bordered by normal faults (Fig. 1). Deformation was achieved in several phases.

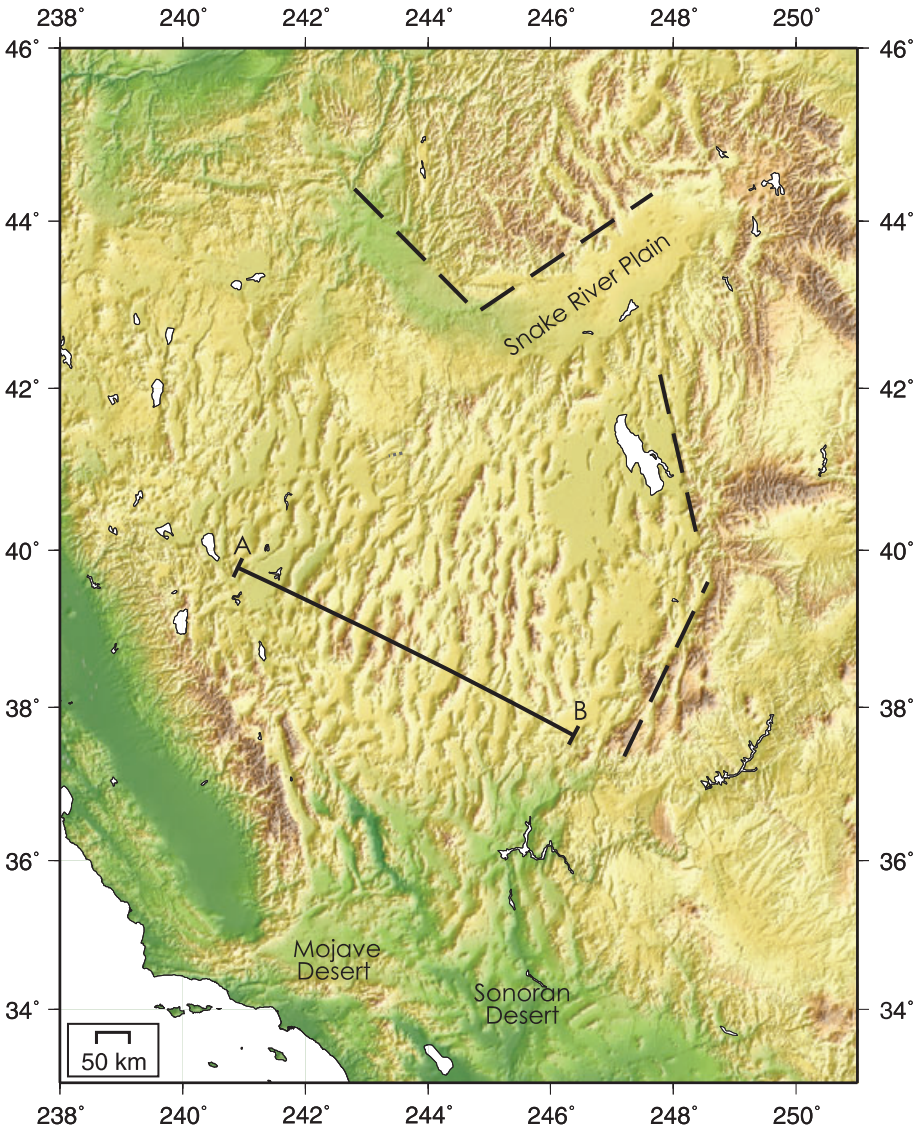

Figure 1. Topographic map of the Basin and Range province. The large area affected by folding may be identified easily from the topographic variations. Lines in large dashes show boundaries that could be compared with the clamped edges of our laboratory experiments.

Extension began around 37 Ma and was oriented WSW–ENE (Zoback & Thompson 1978; Eaton 1982). Around 17 Ma, it switched to a WNW–ESE direction, probably due to the northward migration of the Pacific Plate (Atwater 1970; Zoback & Thompson 1978) and continues today at a rate of a few millimetres per year (Hammond & Thatcher 2004; Hammond & Thatcher 2005). Many exhumed metamorphic domes are observed in the province and are related to folds with characteristic spacings in the 10–20 km range, similar to those of the Aegean (e.g. Fletcher & Bartley 1994; Mancktelow & Pavlis 1994). Part of the complexity of the observed deformations is due to the change of extension direction and the presence of highly extended corridors (Faulds *et al.* 2002). The characteristics of folding have been analysed in detail in several domains of the Basin and Range province. In the central Mojave area, for example, stretching and folding developed at the time of dyke and pluton emplacements about 22–23 Ma (Fletcher & Bartley 1994), during the first extension phase. Tectonite fabrics are consistent with lateral shortening and constrictional strain. The fold axes and stretching lineations are sub-parallel to the WSW–ENE direction, which was the direction of the regional extension at that time (Fletcher & Bartley 1994).

These short summaries show that the Aegean and Basin and Range extension regions exhibit similar features and in particular simultaneous extension in one direction and shortening in the orthogonal direction. Both regions are characterized by large heat flow values of 100 mW m^{-2} or more (Jongsma 1974; Lachenbruch & Sass 1978) and flat Moho discontinuities. They differ in the area affected by folding, however, which is much smaller in the Aegean than in the Basin and Range. As shown later, this difference can be explained by our model.

One final point deals with the intimate relationship between folding and faulting in extension zones (Mancktelow & Pavlis 1994). In the highly extended Colorado corridor, Faulds *et al.* (2002) have described anticlines between listric faults that dip towards one another and synclines between outwardly dipping ones. Such folds are parallel to the strike of the normal faults, indicating that the processes of folding and faulting are genetically related. These two processes were both active at the start of extension and age uncertainties do

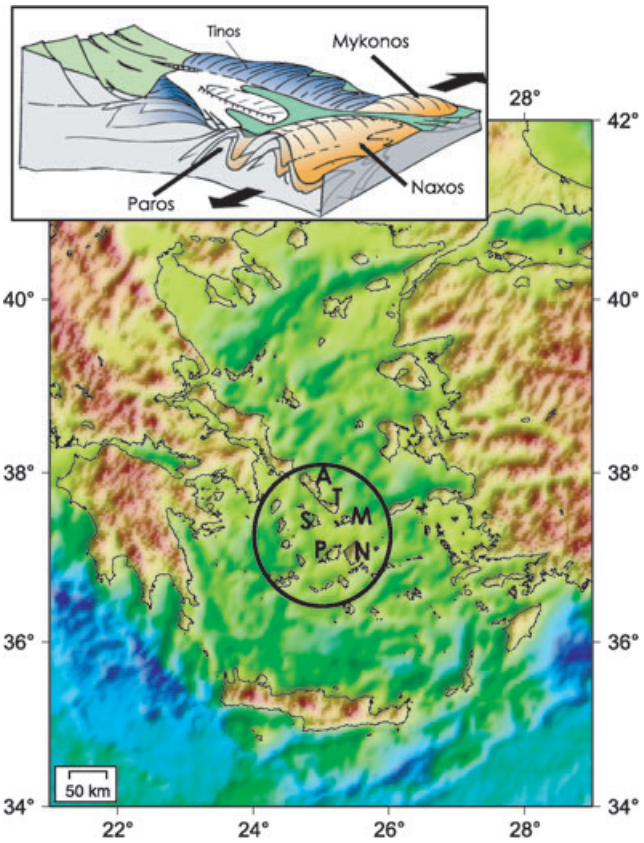

Figure 2. Map of the Aegean, and scheme of the domes observed in the central part of the Aegean Sea (adapted from Jolivet *et al.* 2004). Domes are restricted to the circled area. Paros, Naxos and Mykonos are domes parallel to the extension direction (indicated by large black arrows). Other domes such as Tinos are perpendicular to the direction of extension. They are not studied here.

not allow to separate them in time (Faulds *et al.* 2002). Folding has been attributed to deformation on a fault or within a fault array, involving displacement on a fault plane and/or bending of the fault plane. The fact that folding occurred at the start of extension and was completed in a short amount of time, such that the folds affected deposition of early ash-flow tuffs (Faulds *et al.* 2002), raises two issues. One is that the small amount of extension of an early phase must account for faulting as well as folding. The other issue is why folding stops as extension continues with further displacements on the faults. We shall show in this paper that small amounts of extension can generate extension-parallel folds and faults. Once faulting has occurred, little further folding can occur and most of the extension is accommodated by movements on the faults.

Extension regions are characterized by low-angle detachment faults. From a physical standpoint, such faults cannot be generated by a simple horizontal strain field and necessarily involve flexural stresses (Buck 1988; Spencer & Chase 1989). According to Buck (1988), normal faults are initially generated with dips of about 60°, as predicted by theory, and then rotate due to flexure induced by lateral topographic variations. Spencer & Chase (1989) proposed a different model involving a pre-existing state of flexure, due perhaps to isostically uncompensated Moho reliefs. These two models differ in the time-succession of folding and faulting, but both involve elastic flexure. Flexural stresses also account for the locations of dykes and volcanoes in the Basin and Range (King & Ellis 1990). These observations demonstrate that upper crustal units can sustain significant elastic deformation.

3 FOLDING OF A THIN ELASTIC SHEET UNDER EXTENSION: LABORATORY STUDY

Although it is well established that the upper crust breaks or yields after small amounts of strain, it is worthwhile to study what happens before the onset of faulting, when deformation proceeds in an elastic regime. We study folding that develops in thin elastic sheets under extension and use the theoretical framework provided by Cerda *et al.* (2002). We discuss later the elastic sheet approximation in relation to the more complex rheological profile of continental lithosphere. In their study, Cerda *et al.* (2002) report on measurements of fold wavelength and we complement their observations with data on the amplitude of folds. We also investigate other characteristics of the deformation, focussing on parts where no folding occurs. We finally document how folding proceeds in more complicated geometrical configurations.

3.1 Fold characteristics

Large deformations of elastic thin sheets are governed by a set of non-linear differential equations known as the Föppl-von Karman equations. Analytical solutions are available in a few cases only (Landau & Lifshitz 1986) and numerical solutions are hard to implement due to high-order differentials and the changes of domain dimensions that must be accounted for (Friedl *et al.* 2000). Simple scaling laws for deformation under extension have been derived by Cerda *et al.* (2002) and Cerda & Mahadevan (2003). They consider an isotropic elastic sheet of thickness h, width W and length L. The theory is only valid for thin elastic sheets, such that h/L and h/W are $\ll 1$, which is valid for geological cases.

In the reference set up, a rectangular elastic sheet is subjected to a uniaxial extensional stress parallel to the two free boundaries in the x-direction, by moving apart the two other boundaries that are kept clamped (Fig. 3). The sheet develops periodic folds with axes that are parallel to the extension in a central region even for very small amounts of extension (Figs 3 and 4). The sheet remains flat near its two clamped boundaries (Fig. 5). As shown in Appendix A, minimizing the energy for bending and stretching leads to the following scaling laws for the amplitude A and wavelength λ of the folds:

$$A = (\nu L h)^{\frac{1}{2}} \left[\frac{16\gamma}{3\pi^2(1-\nu^2)}\right]^{\frac{1}{4}}, \tag{1}$$

$$\lambda = \frac{(2\pi L h)^{\frac{1}{2}}}{[3(1-\nu^2)\gamma]^{\frac{1}{4}}}, \tag{2}$$

where γ is the amount of extension and ν is the Poisson's ratio for the sheet. Note that λ does not depend on the width of the sheet, in contrast to buckling under compression (Turcotte & Schubert 1982).

To establish the validity of these scaling laws, we have used two different materials (PolyEthylene and PVC) and different sheet thicknesses (Table 1). We have also worked with sheets of different sizes to provide data on the dimensions of regions affected by folding and regions that remain flat near the clamped boundaries. We determined the amplitude and wavelength of the folds with a

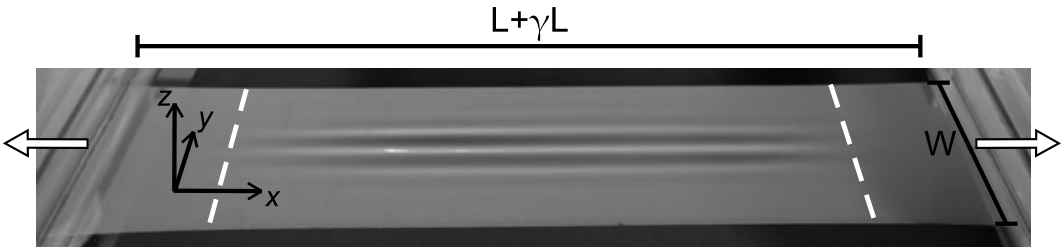

Figure 3. Wrinkles in a polyethylene sheet stretched in the x-direction. The dashed lines mark the boundaries of flat zones near the clamped boundaries of the sheet.

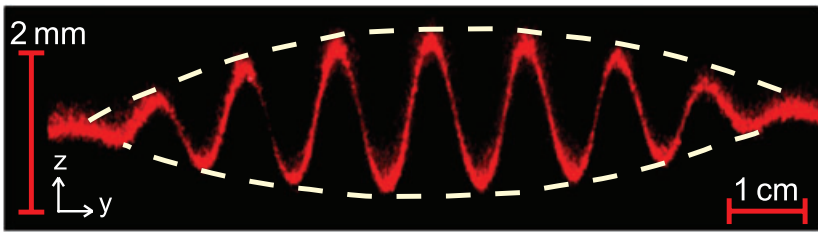

Figure 4. Deflection of a linear laser beam perpendicular to the fold axes, at equal distances from the clamped edges. The horizontal scale is larger than the vertical one. Folds are fully developed in the central part of the sheet and decrease in amplitude towards the lateral edges of the sheet.

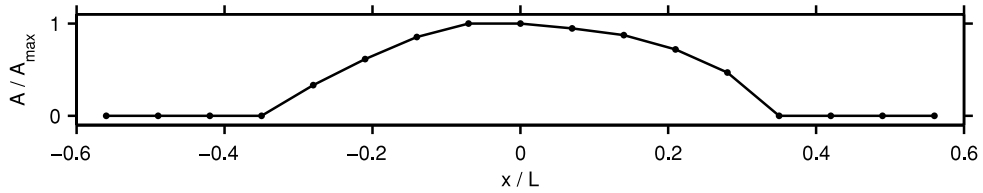

Figure 5. Longitudinal profile of a fold along its apex. Dots are amplitude measurements made with a laser beam at different distances from the clamped edges.

Table 1. Dimensions of the stretched sheets.

Thickness, h	PE	30, 80, 100 and 150 μm
	PVC	50 and 80 μm
Width, W		10–22 cm
Length, L		24.8–33 cm
Aspect ratio (W/L)		0.38–0.75

planar laser sheet shone in the extension direction at a low incidence angle relative to the horizontal (Fig. 4). Folds appear for very small amounts of stretching. For the dimensions of the experimental apparatus and elastic sheets, the critical amount of extension that is required for folding cannot be determined because we observed folding for all values of the amount of extension that could be measured, which were as small as 0.5 per cent. The amplitude of the folds increases away from the free lateral edges of the sheet and is maximum in the central part of the sheet (Fig. 4). Folds do not develop in the vicinity of the clamped boundaries which prevent lateral shortening.

The maximum amplitude and wavelength of the folds (i.e. in the central part of the sheet) follow the theoretical scaling laws (eqs 1 and 2) up to about 10 per cent of extension. For further stretching, the measured wavelength remains consistent with the scaling law, but the amplitude falls below the predicted value (Fig. 6).

We have also tested the validity of the scaling laws using the total amount of shortening at mid-distance from the clamped boundaries. The shortening is due to folding, and hence can be written as

$$\left|\frac{\Delta W}{W}\right| = \frac{l-\lambda}{l}, \tag{3}$$

where l is the length of the sheet along one fold of wavelength λ (Fig. 7)

$$l = \int_0^{\lambda} \mathrm{d}s, \tag{4}$$

where s is the curvilinear abscissa such that $\mathrm{d}s = \sqrt{\mathrm{d}y^2 + \mathrm{d}\zeta^2}$ (Fig. 7). Assuming that the folds are sinusoidal in shape, such that $\zeta = A\sin(\frac{2\pi y}{\lambda})$, and replacing A and λ by their expressions, we finally obtain

$$\left|\frac{\Delta W}{W}\right| = \frac{2\nu\gamma}{1+2\nu\gamma}. \tag{5}$$

The agreement between predicted and measured amounts of shortening is excellent for $\gamma < 10$ per cent (Fig. 8). For further stretching, the observed shortening is slightly less than predicted, which is consistent with the amplitude of folds being smaller than predicted.

3.2 Undeformed regions near rigid bounding blocks

We have studied the characteristics of the undeformed regions near the two clamped boundaries (Fig. 3). Near these boundaries and away from the lateral edges of the sheet, where no stress is applied, the sheet cannot contract laterally and the normal stress in the

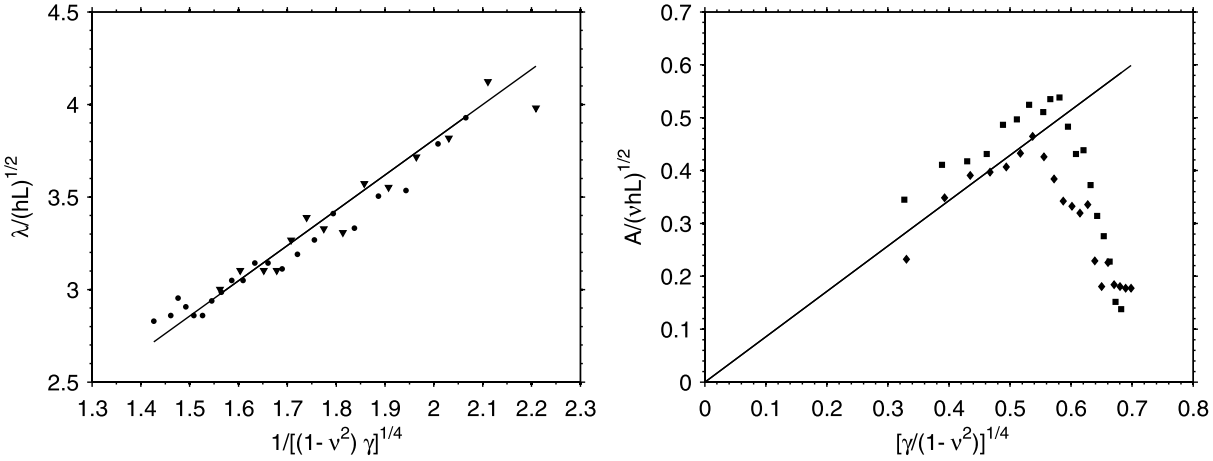

Figure 6. Dimensionless wavelength (left) and amplitude (right) as a function of the amount of extension. Circles: PE, $h = 150$ μm, $L = 27$ cm, $W = 18$ cm. Triangles: PVC, $h = 80$ μm, $L = 30$ cm, $W = 20$ cm. Squares: PE, $h = 80$ μm, $L = 30$ cm, $W = 16.5$ cm. Diamonds: PVC, $h = 80$ μm, $L = 30$ cm, $W = 19$ cm. The solid lines show the scaling laws.

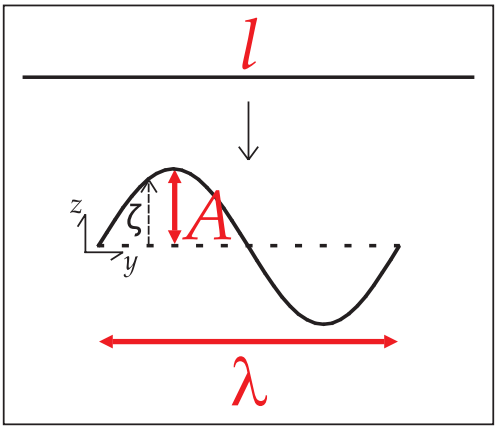

Figure 7. Notations used in Section 3.1.

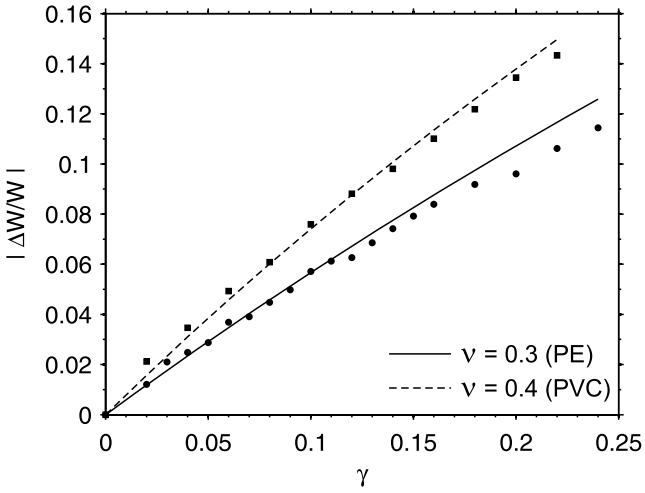

Figure 8. Lateral shortening versus amount of extension for a thin elastic sheet. Squares: PVC, $h = 50$ μm, $L = 27.5$ cm, $W = 13.9$ cm. Circles: PE, $h = 30$ μm, $L = 26.5$ cm, $W = 10.5$ cm. The solid and dashed lines show the scaling laws for PVC and PE, respectively.

direction perpendicular to extension, σ_{yy}, is in tension. At some distance to the rigid boundaries (in the x-direction) noted δ, this stress changes sign as the sheet is subjected to folding, which induces a state of compression in the middle of the sheet (Friedl *et al.* 2000). This distance defines the extent of the unfolded region. We have measured this extent using the same illumination technique as that for the folds. These measurements are not very accurate, especially at small amounts of extension because of the very small amplitude of the folds. Scaled to the large width of the sheet, however, such uncertainties are small. From the data, we can clearly distinguish between two behaviours. For amounts of extension that are less than 10 per cent, δ/W, the dimensionless extent of the undeformed regions remains approximately constant at a value of about 0.35, independently of the sheet aspect ratio W/L (Fig. 9). For larger amounts of extension, the unfolded region takes up an increasing part of the sheet.

According to these results, the unfolded regions adjacent to the rigid boundaries take a total length of $2\delta = (2 \times 0.35)\ W = 0.7W$. Thus, if the total length of the sheet is less than $0.7 \times W$, we expect that no folding occurs. Indeed, we observed that the elastic sheet does not fold visibly under stretching if $L \leq 0.75 \times W$.

3.3 Large amounts of extension

Based on our observations, we can interpret the behaviour of the stretched sheet as follows. For amounts of extension that are less than about 10 per cent, deformation is purely elastic and perfectly described by the scaling laws given earlier. For larger amounts of extension, plastic deformation near the clamped boundaries becomes significant and takes up an increasing part of the sheet, reducing the area available for shortening and folding. As a consequence, the folds are not fully developed. Their wavelength still follows the elastic law, but their amplitude decreases with increasing extension. The amplitude of folds eventually becomes negligible when deformation is in a plastic regime everywhere.

For the experimental materials of this study, plastic deformation becomes significant at strains of about 10 per cent. This was established by determining the amount of residual deformation when stretching is relieved. This was also reflected in the reduced amplitude of folds and the concomitant reduction in the amount of

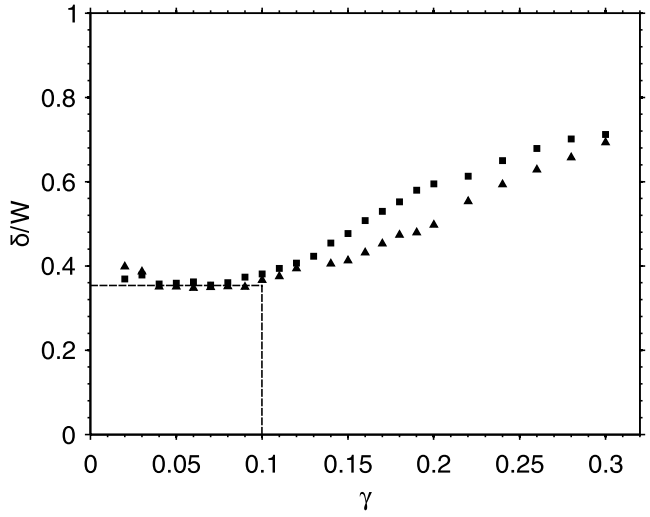

Figure 9. Dimensionless extent of flat zones in the *Ox*-direction against the amount of extension. Squares: PE, $h = 100$ μm, $L = 26.5$ cm, $W = 10$ cm. Triangles: PE, $h = 100$ μm, $L = 26.5$ cm, $W = 15$ cm.

lateral shortening that occurs. As shown by eq. (5), the amount of shortening is a simple function of the amount of extension in the elastic regime, and the breakdown of this relationship is a straightforward indication that deformation is no longer elastic. For geological cases, we are interested in early stages of deformation in an elastic regime. In Section 4, we extend the results for an isolated elastic sheet to cases involving an elastic layer underlain by material deforming either elastically, but with different elastic properties, or viscously.

3.4 Geometrical constraints on deformation

So far, we have studied extension in a simple configuration, such that the elastic sheet has free boundaries parallel to the extension direction and rigid boundaries perpendicular to it. In the Earth, such geometrical simplicity is unlikely. Because of the inherently 3-D nature of the strain field, we expect that the deformation field is sensitive to the shape of the elastic sheet in relation to the extension direction. We investigate the consequences using a series of experiments with different configurations. We have restricted our study to generic cases which illustrate a few key features.

In a first set of experiments, we have considered a V-shaped rigid boundary at one end of the sheet. This rigid boundary partially encapsulates the elastic sheet and prevents shortening. We found indeed that the encapsulated region does not fold at all and enlarges the flat region at the end of the sheet (Fig. 10). We have also considered an extreme case. A rectangular sheet had four rigid edges (i.e. clamped boundaries) with small adjustment zones at the four vertices between two adjacent rigid boundaries. This sheet was stretched in a direction parallel to one side of the rectangle, as before, by moving the other two rigid boundaries. The adjustment zones allowed folding perpendicular to extension with wavelengths and amplitudes that were similar to those for free lateral boundaries (Fig. 11). The reason for this is that folding can develop even with very small amounts of shortening, and hence can take advantage of the shortening allowed by the adjustment zones. Complex deformation occurred near the lateral rigid boundaries, involving two conjugate folds that were oblique to the extension direction. Another difference with the reference experiment of Fig. 3 was in the shape and size of the undeformed region next to the moving boundaries.

In a second set of experiments, we considered elastic sheets whose boundaries were not aligned with the stretching or shortening directions. This generates complicated geometrical constraints on shortening, which should occur at a right angle to the extension in a global sense but also at a right angle to free lateral edges. If the free lateral boundaries are at an angle to the extension (Fig. 12), folding occurs in the middle of the sheet, but the folds are at an angle, noted α, to the extension, due to the two conflicting constraints on shortening. With increasing amounts of extension, the folds tend to align themselves to the free boundaries, illustrating the dominant control on the shortening direction. In a final set-up, the free lateral boundaries were parallel to the stretching direction but the rigid boundaries were not perpendicular to it. In this case, the rigid boundaries are at odds with the extension and shortening directions. We observed two types of folds in different parts of the sheet. Shortening proceeds in the middle of the sheet but the folds were again not aligned with the extension (Fig. 13). Angle α also varies as the amount of extension is augmented. Near each moving rigid boundary, folding occurs in a small triangular area with axes that are parallel to the extension. In these end zones, the amount of shortening varies along strike, which causes a slight rotation of the folds in the middle part of the sheet.

These experiments illustrate that folds may develop at an angle to the extension direction due to geometrical constraints on deformation and may rotate as the amount of extension increases.

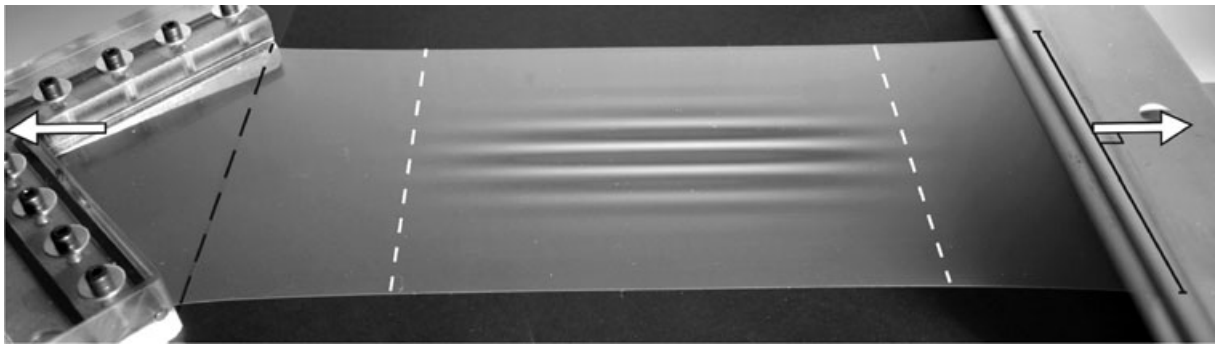

Figure 10. Stretching of a PE sheet with one straight rigid boundary at one end and two orthogonal rigid boundaries at the other end. The large white arrows show the stretching direction. The wrinkling pattern is similar as in Fig. 3. The white dashed lines are the boundaries of the flat regions. The area defined by the V-shaped rigid boundary and the dashed black line is too constrained to wrinkle. The sheet dimensions are $h = 80$ μm, $L_{max} = 33$ cm, $W = 14$ cm.

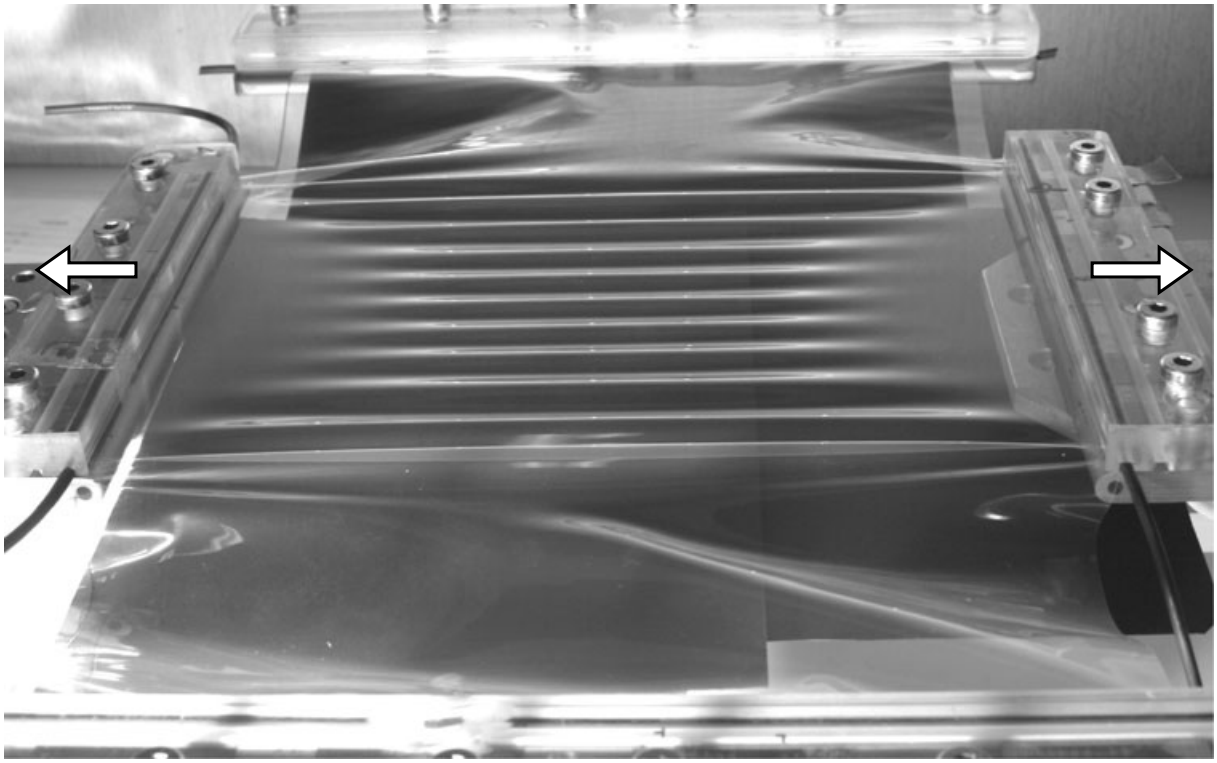

Figure 11. Stretching of a PE sheet with four clamped edges. White arrows show the stretching direction. The sheet dimensions are $h = 100$ μm, $L = 28$ cm, $W_{\text{tot}} = 43$ cm. A width of 21 cm is clamped.

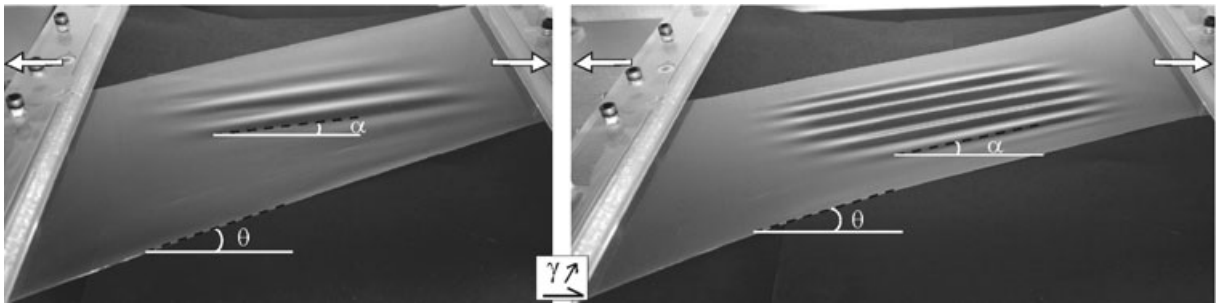

Figure 12. Stretching of a PE sheet with clamped edges normal to the stretching direction (indicated by the large white arrows), and free edges forming an angle θ with the stretching direction. The axis of the wrinkles tends to align parallel to the free edges as the amount of extension increases. The sheet dimensions are $h = 80$ μm, $L = 30$ cm, $W = 16$ cm.

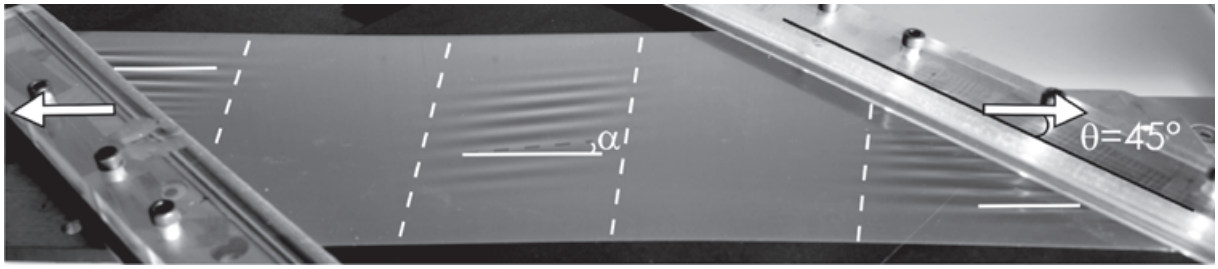

Figure 13. Stretching of a PE sheet with clamped edges at 45° of the stretching direction (indicated by the large white arrows). Two families of wrinkles can be distinguished. Near the clamped edges, wrinkles are parallel to the stretching direction. In the central part of the sheet, they form an angle θ with the stretching direction. This angle varies with the amount of extension. The sheet dimensions are $h = 80$ μm, $L = 30$ cm, $W = 16$ cm.

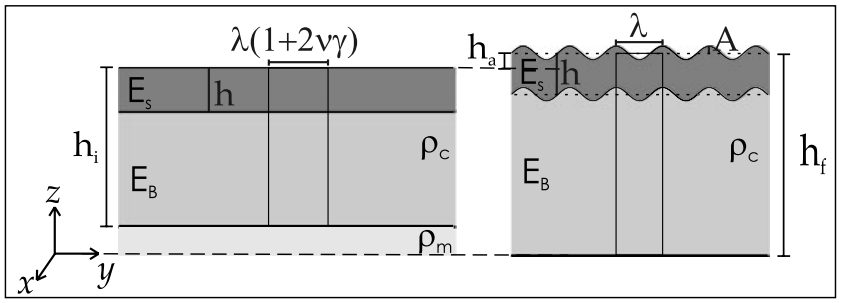

Figure 14. Scheme of the model studied in Section 4.1. Left-hand panel: reference state, right-hand panel: wrinkled state. Rectangles of dimensions $\lambda(1 + 2\nu\gamma)$, h_i and λ, h_f define zones of equal masses.

4 THEORETICAL MODEL FOR THE CHARACTERISTICS OF FOLDS

4.1 Energy minimization

To adapt the theory developed before to terrestrial deformations, we need to take into account several additional effects. One such effect involves gravity and the changes of potential energy that are associated with changes of topography. Such changes are negligible at the scale of the laboratory, but cannot be ignored in geological cases. We must also account for the fact that, on Earth, the thin elastic plate is a superficial layer, underlain by a thicker 'substrate' (Fig. 14). For the large crustal temperatures that are implied by the small effective elastic thickness and large heat flow values, Young's modulus decreases significantly with depth, such that one may approximate this rheological stratification by a strong layer overlying a weaker elastic substrate. Depending on the thermal structure, this substrate may also behave as viscous material.

The total energy variation when such a system is stretched is the sum of the following.

(i) A variation of potential energy. It is calculated assuming that the wavelength of the wrinkles is too small for them to be isostatically compensated, as observed. We only consider a large-scale compensation due to shortening and the induced crustal thickening (Fig. 14).

(ii) The bending energy of the superficial elastic layer.

(iii) The stretching energy of the superficial elastic layer.

(iv) If the substrate is viscous, the energy dissipation depends on the deformation velocity. As the processes we study are slow, such viscous dissipation may be neglected.

(v) If the substrate is considered as elastic, an energy contribution due to the deformation of the substrate. In a substrate thick relatively to the surface layer, the amplitude of superficial deformations decays exponentially with depth, with a characteristic length scale equal to the wavelength of the folds. We assume that the thickness of the substrate is greater than the wavelength of the folds, and hence treat it as a half-space.

A geometrical constraint of inextensibility in the shortening direction is imposed when minimizing the energy. All the calculations are detailed in Appendix B.

For a viscous substrate such that dissipation due to lower crustal flow is negligible, the energy minimization leads to

$$\frac{3}{4}\rho_c g\lambda^4 + \left(\frac{C}{\Delta} + E_s\gamma h\right)\lambda^2 - E_s h^3 = 0, \tag{6}$$

where C and Δ are defined later. For an elastic substrate, we obtain

$$\frac{3}{4}\rho_c g\lambda^4 + 2E_b\lambda^3 + \left(\frac{C}{\Delta} + E_s\gamma h\right)\lambda^2 - E_s h^3 = 0, \tag{7}$$

with E_s, the Young's modulus of the surface layer, and E_b the Young's modulus of the substrate.

In both cases, Δ is the transverse shortening (eq. 5)

$$\Delta = \frac{2\nu\gamma}{1 + 2\nu\gamma}, \tag{8}$$

and

$$C = \rho_c g\nu\gamma h_i^2 (1 + 2\nu\gamma)\left(1 - 2\frac{\rho_c}{\rho_m}\right) \tag{9}$$

(see Fig. 14 for the definition of h_i).

4.2 Numerical results

The new equations do not imply large departures from the simple scaling laws given by eqs (1) and (2). The wavelength and amplitude of the folds are moderately sensitive to the elastic thickness h because they scale approximately with $h^{1/2}$. This parameter is in a 5–15 km range in the Basin and Range according to Lowry & Smith (1994) and we adopt a value of 10 km for the sake of example. We take an initial crust thickness $h_i = 35$ km, Young's modulus $E_s = 30$ GPa and $\rho_c = 2700\,\mathrm{kg\,m^{-3}}$ for the crust and $\rho_m = 3300\,\mathrm{kg\,m^{-3}}$ for the mantle (Table 2). Solutions were obtained for the simple geometrical configuration of a rectangular elastic sheet with edges that are aligned with and perpendicular to the extension direction, which is not always appropriate. However, our laboratory experiments show that the wavelength and amplitude of the folds remain of the same order of magnitude for other configurations. This is simply due to the inextensibility constraint in the folded region. We thus use $A \sim \lambda\sqrt{\Delta}$.

Fig. 15 shows the wavelength and amplitude as a function of the amount of extension. Even for very low extension factors, folds with a significant amplitude are generated by the stretching. For a viscous substrate, which seems appropriate for high heat flux regions such as the Aegean and the Basin and Range, for 3 per cent of extension

Table 2. Geological parameter values.

h	Elastic thickness	10 km
h_i	Crustal thickness	35 km
ρ_c	Crustal density	$2700\,\mathrm{kg\,m^{-3}}$
ρ_m	Mantle density	$3300\,\mathrm{kg\,m^{-3}}$
E_s	Young's modulus, surface layer	30 GPa
E_b	Young's modulus, elastic substrate	1 GPa

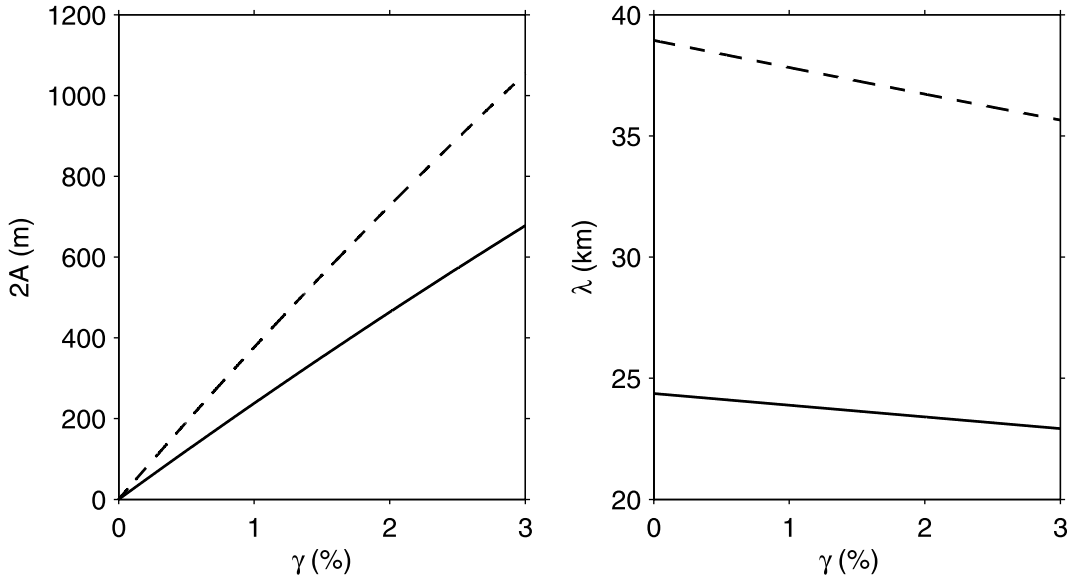

Figure 15. Amplitude (left-hand panel) and wavelength (right-hand panel) versus the amount of extension γ. Solid lines are for the model with an elastic substrate, dashed lines are for a viscous substrate. The parameter values used in the calculations are given in Section 4.2.

folds have an amplitude of 500 m, and a wavelength of 36 km. If we consider a weak elastic substrate, with a small Young's modulus $E_b = 1$ GPa for example, eq. (7) leads to an amplitude of 300 m and a wavelength of 23 km. The amount of extension that has been chosen for these calculations may be larger than in reality and we discuss this point later.

5 DISCUSSION

5.1 Comparison with observations

Large-scale folds that form metamorphic domes and their internal structure clearly indicate ductile deformation. We propose that ductile extension-perpendicular folding was imposed by the folding of a thin superficial elastic layer, and that folds were later exhumed. In this model, the lateral shortening which generates the folds results from a combination of the longitudinal stretching and the boundary conditions (Friedl *et al.* 2000): no external compression in a direction perpendicular to extension is required. This is consistent with the analysis of Fletcher & Bartley (1994). On the contrary, folding of a ductile layer only (no elastic layer) would not be achievable under such a regime: ductile folding may only proceed if some compression is applied (Schmalholz 2008).

In geological reality, the amount of extension may not be known with great accuracy. The main result is perhaps that the wavelength of the elastic folding is not very sensitive to this variable and takes values of a few tens of kilometres for all reasonable combination of input parameters. Another important result is that folding does not require large amounts of extension, as shown by the laboratory experiments, and by Fig. 15. Structures with a significant amplitude are formed even for amounts of extension that are less than 1 per cent.

The wavelength of folds is predicted to be in the 20–40 km range depending on the behaviour of the substrate, which is consistent with the observations of metamorphic domes in both the Aegean and the Basin and Range. Similar folds have been mapped in the Norwegian Caledonides (Chauvet & Séranne 1994). In the Basin and Range, Mancktelow & Pavlis (1994) observe that the amplitude of the folds decreases and the wavelength increases for progressively younger structures. Assuming that the amount of extension increases with time, this observation can be recast as an increase in the amplitude of folds and a decrease of the wavelength of folds as the amount of extension is increased, which is consistent with the theoretical expectations.

In this model, the characteristics of folds are essentially set by the elastic layer. The wavelength λ that is found has important implications for deformation in the lower crust. Horizontal stress variations are generated over that same wavelength at the top of the substrate below the elastic layer and decay over an e-folding depth of $\lambda/(2\pi)$, as shown by Turcotte & Schubert (1982). This e-folding depth is therefore less than 10 km, implying that horizontal stress variations are very small at the base of the crust, which explains why the Moho discontinuity is not deflected. In other words, the Moho remains horizontal because of the wavelength that is selected.

In the Aegean, the setting is relatively simple: the extension direction has not varied through time, and the geometry of the Aegean Sea can be roughly approximated by a rectangle with long sides parallel to the stretching direction. This allows a straightforward comparison with laboratory experiments. Extension parallel folds that form the domes of Naxos, Paros and Mykonos (Fig. 2) are located in the central part of the extended region, which is consistent with the experimental observations. In the Aegean, the aspect ratio of the extension zone W/L was probably about 1, so that we expect that the folded area is small and involves a small number of folds, as observed.

In the Basin and Range, the geometry of the extended domain is more complex than in the Aegean, and the extension direction has changed with time, from WSW–ENE to WNW–ESE. The large dimensions of this province prevent generalizations of the simple physical model. Mineralogical dating indicates that extension-parallel folds that formed many metamorphic domes were generated in early stages of extension (Fletcher & Bartley 1994). The topographic highs and lows are due to displacements along normal faults that are nearly perpendicular to the stretching. We suggest that some of these faults may have localized along folds that were generated in the first extension phase and elaborate on this in a

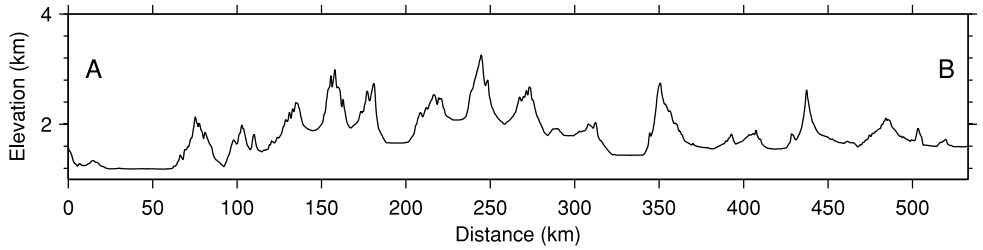

Figure 16. Topographic profile AB across the Basin and Range province, as defined on Fig. 1.

separate section. We note that many aspects of the Basin and Range topographic structures are consistent with those of elastic folding. Their strike is subparallel to the WSW–ENE extension direction. It slightly varies across the region, which can also be compared to laboratory observations (Section 3.4). The Moho is flat beneath the province (Klemperer *et al.* 1986; Gans 1987). The amplitude of the surface undulations is maximum at the centre and decreases towards the edges of the province (Fig. 16), as in the experiments (Fig. 4). Another interesting feature is the Snake River Plain at the northern end of the province, which was subjected to the same regional extension (Parsons *et al.* 1998), but which has remained unfolded. This part of the province lies against rigid boundaries where neither extension nor shortening are allowed.

5.2 Towards faulting

If the stress field driving the deformation is uniaxial along the extension direction, as proposed by Fletcher & Bartley (1994), classical theoretical arguments predict faulting in a direction perpendicular to that of stretching (Spencer & Chase 1989). According to Buck (1988) and Spencer & Chase (1989), such faults develop into the prominent low-angle detachments that characterize extension zones. In the Aegean and in the Basin and Range, however, there is also another set of faults that are parallel to fold axes and to the stretching direction (Fletcher & Bartley 1994; Janecke *et al.* 1998; Faulds *et al.* 2002).

Folding of the elastic upper crustal layer may induce failure in the extension direction, but it requires a minimum amount of folding and hence a minimum amount of stretching. One must therefore consider two different extension thresholds for the two types of faulting that may occur: one for extension-parallel faults induced by folding and the other for extension-perpendicular faults. Clearly, if the former is larger than the latter, extension gets accommodated mostly by extension-perpendicular faults with minor extension-parallel folds and no extension-parallel faults. We use the Mohr–Coulomb criterion, such that the tangential stress τ exceeds a critical value given by $\tau = \mu p + C$, where μ is the friction coefficient, C is cohesion and p the normal stress, respectively. For the elastic plate, we write the force and momentum equilibrium equations in the Oyz plane using beam theory (Landau & Lifshitz 1986):

$$\begin{cases} -\dfrac{\mathrm{d}p}{\mathrm{d}y} + \dfrac{\mathrm{d}^2\zeta}{\mathrm{d}y^2}\tau - \rho g \dfrac{\mathrm{d}\zeta}{\mathrm{d}y} = 0, \\ p\dfrac{\mathrm{d}^2\zeta}{\mathrm{d}y^2} + \dfrac{\mathrm{d}\tau}{\mathrm{d}y} + \rho g = 0, \\ \dfrac{\mathrm{d}M}{\mathrm{d}y} = h\tau, \end{cases} \tag{10}$$

where ζ is the shape of folds (Fig. 7), p is the average normal stress through the plate, τ is the tangential stress and M is the bending moment.

In a fold, half of the elastic layer is in compression and the other half is in extension. On the contrary, the tangential stress is applied over the whole plate thickness. Thus, faults will localize where the tangential stress is maximum. The tangential stress τ can be derived from the momentum equilibrium equation

$$\tau = \frac{D}{h}\frac{\mathrm{d}^3\zeta}{\mathrm{d}y^3}. \tag{11}$$

Assuming that the folds are sinusoidal in shape, we obtain

$$\tau = -\frac{2\pi^3 E h^2 A}{3\lambda^3(1-\nu^2)}\cos\left(\frac{2\pi y}{\lambda}\right). \tag{12}$$

The absolute value of the tangential stress is maximum at the inflection points of the folds, between the top (the range) and the base (the basin) of the fold. The average normal stress p is deduced by integrating the first equation

$$p = \rho g\left(\frac{h}{2} - A\sin\left(\frac{2\pi y}{\lambda}\right)\right) + \frac{D}{2h}A^2\left(\frac{2\pi}{\lambda}\right)^4\sin^2\left(\frac{2\pi y}{\lambda}\right). \tag{13}$$

At the inflection point of the folds, $p = \frac{\rho g h}{2}$. Fig. 17 shows the ratio $(\tau - C)/p$ as a function of the extension factor. For a friction coefficient $\mu = 0.65$ and a viscous substrate, rupture in a direction parallel to extension occurs after ~0.5 per cent of extension.

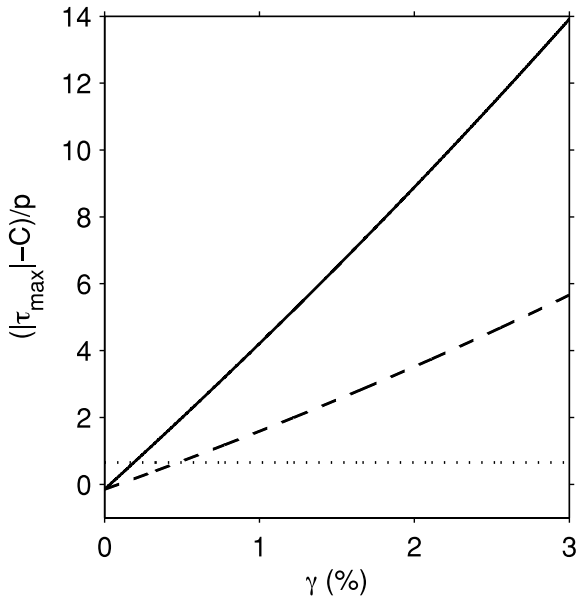

Figure 17. Stress ratio in a folded elastic sheet versus the amount of extension γ. Solid lines are for the model with an elastic substrate, dashed lines are for a viscous substrate. The parameter values used in the calculations are given in the text, except for cohesion C which is 20 MPa. The dotted line shows the value of the friction coefficient $\mu = 0.65$. Faulting occurs when the stress ratio becomes larger than μ.

Rupture may also occur in conjugate strike-slip faults at an angle to the uniaxial extensional stress field (Fletcher & Bartley 1994) or steep normal faults perpendicular to the stretching (Spencer & Chase 1989). This occurs when the regional stress has reached a value

$$\sigma_R = \frac{2\,(\mu\rho g h + 2C)}{3\mu + \sqrt{3}}. \tag{14}$$

For a horizontal uniaxial stress field, the corresponding extension factor is simply equal to this stress divided by Young's modulus E. We obtain a critical extension factor of 0.8 per cent, which is larger than that for faulting due to folding.

We conclude that extension-parallel faulting occurs first, before rupture in other directions. This is an important result for the model that is proposed for the Basin and Range province. The fault array bordering basins and ranges may have localized along folds formed during the initial WSW–ENE extension phase, subparallel to the extension direction at that time. In the more recent phase of WNW–ESE extension, spreading in the direction of extension could have been accommodated by displacements across the already existing fault array.

5.3 Elastic thickness

In the Earth, the elastic thickness must be understood as an effective thickness which depends on the thermal structure as well as the magnitude and sign (i.e. in tension or compression) of the deviatoric strain and stress (Goetze & Evans 1979). The effective thickness is smaller in tension than in compression because rocks fail at lower stress levels in tension than in compression. The mechanism invoked in this paper relies on tension in the x-direction and zero applied stress in the y-direction. Folding is due to shortening in the y-direction with a total amount that depends only on the amount of extension and Poisson's ratio (eq. 5). The elastic thickness for folding involves both tension and compression on either side of the neutral surface (Goetze & Evans 1979). In geological reality, this effective thickness is not the same as that for horizontal extension due to the different deviatoric stress distributions involved. This difference has no bearing on the analysis for folding, which relies on the amount of extension and a purely geometrical constraint, and not on the stresses involved.

Folding in an elastic regime is traditionally ruled out on the grounds that it requires large stresses that are not available in nature (Turcotte & Schubert 1982). This issue is discussed by Marques & Podladchikov (2009), who provide some counter-arguments. These authors emphasize that elastic deformation does occur for small amounts of strain and that it may affect later phases of deformation. As regards the conditions for a given amount of strain, a key variable is the elastic thickness because stresses get concentrated in the mechanically strong upper crustal material and hence in the elastic layer (Marques & Podladchikov 2009): for a given total driving force, the smaller the elastic thickness is the larger the extensional stresses are. In regions of extension, we expect a small elastic thickness in association with high heat flow, due to both stretching at the lithospheric scale and magma intrusions in the crust. Analysis of topography and gravity anomalies confirm that the effective elastic thickness is small in these regions, in a range of 5–15 km (Lowry & Smith 1994). In such conditions, the small amounts of deformation that are needed for folding require small applied stresses and hence a small total driving force.

We have already commented on the lack of isostatic compensation for the topography in both the Aegean and the Basin and Range. For periodic undulations of topography with wavelength λ, relaxation in a viscous material occurs over a characteristic time $\Delta t \approx 4\pi\mu_c/(\rho_c g\lambda)$, where μ_c is the effective viscosity. For $\lambda = 40$ km and an effective viscosity that is less than 10^{22} Pa s (e.g. Kruse *et al.* 1991; Kaufman & Royden 1994; McKenzie *et al.* 2000), it is not possible to maintain basin-and-range topography for more than 3 Ma. Thus, such topography must be supported elastically.

6 CONCLUSIONS

In initial phases of extension, the total strain is small and there must be an elastic component to the deformation. Our analysis suggests that this has important consequences for further deformation at larger values of displacement and strain. We have shown that the stretching of a thin elastic plate leads to folding and have verified the validity of simple scaling laws using laboratory experiments. Such deformations are significant even for amounts of extension that are as small as one percent or less. In the case of the longitudinal extension of a rectangular plate, folds are oriented parallel to the stretching direction. For more complex configurations, the fold axes may not be perfectly aligned with the extension direction and may rotate slightly with increasing amounts of extension.

We propose that metamorphic domes result from a ductile folding imposed by the elastic deformation of an upper crustal layer in response to stretching. An energy minimization calculation allows us to estimate the wavelength and amplitude of the folds in the case of the Earth's crust. We obtain values comparable to those of extension-parallel folds that are observed in metamorphic domes in continental extended terranes. We show that even though the amount of extension which occurs before faulting is small, it is sufficient to form significant undulations of Earth's surface. This model explains the geometry of the structures observed in the Aegean Sea and in the Basin and Range, as well as their main characteristics. It also explains why the induced topography is not isostatically compensated and why the Moho remains flat in such regions. Finally, the model accounts for some of the topographic features of the Basin and Range province, which may have been set up by the same process.

ACKNOWLEDGMENTS

We thank the Editor, A. Agnon and S. Schmalholz for their useful comments, criticisms and suggestions which helped us improve the manuscript.

REFERENCES

Atwater, T., 1970. Implications of plate tectonics for the cenozoic tectonic evolution of Western North America, *GSA Bull.,* **81,** 3513–3536.

Avigad, D., Ziv, A. & Garfunkel, Z., 2001. Ductile and brittle shortening, extension parallel folds and maintenance of crustal thickness in the Central Aegean, *Tectonics,* **20**(2), 277–287.

Benes, V. & Davy, P., 1996. Modes of continental lithospheric extension: experimental verification of strain localization processes, *Tectonophysics,* **254,** 69–87.

Buck, W.R., 1988. Flexural rotation of normal faults, *Tectonics,* **7**(5), 959–973.

Buck, W.R., 1991. Modes of continental lithospheric extension, *J. geophys. Res.,* **96**(B12), 20 161–20 178.

Cerda, E. & Mahadevan, L., 2003. Geometry and physics of wrinkling, *Phys. Rev. Lett.,* **90**(7), doi:10.1103/PhysRevLett.90.074302.

Cerda, E., Ravi-Chandar, K. & Mahadevan, L., 2002. Wrinkling of an elastic sheet under tension, *Nature,* **419,** 579–580.

Chauvet, A. & Séranne, M., 1994. Extension-parallel folding in the Scandinavian Caledonides: implications for late-orogenic processes, *Tectonophysics,* **238,** 31–54.

Corti, G., 2005. Dynamics of periodic instabilities during stretching of the continental lithosphere: view from centrifuge models and comparison with natural examples, *Tectonics,* **24,** doi:10.1029/2004TC001739.

Dewey, J.F., 1988. Extensional collapse of orogens, *Tectonics,* **7,** 1123–1139.

Eaton, G.P., 1980. Geophysical and geological characteristics of the crust of the basin and range province, in *Continental Tectonics,* pp. 96–113, eds, Burchfiel, B.C., Oliver, J.E. & Silver, L.T., National Academy of Science, Washington, DC.

Eaton, G.P., 1982. The Basin and Range Province: origin and tectonic significance, *Ann. Rev. Earth planet. Sci.,* **10,** 409–440.

Faulds, J.E., Olson, E.L., Harlan, S.S. & McIntosh, W.C., 2002. Miocene extension and fault-related folding in the Highland Range, southern Nevada: a three-dimensional perspective, *J. Struct. Geol.,* **24,** 861–886.

Fletcher, J.M. & Bartley, J.M., 1994. Constrictional strain in a non-coaxial shear zone: implications for fold and rock fabric development, central Mojave metamorphic core complex, California, *J. Struct. Geol.,* **16**(4), 555–570.

Fletcher, J.M., Bartley, J.M., Martin, M.W., Glazner, A. & Walker, J.D., 1995. Large-magnitude continental extension: an example from the central Mojave metamorphic core complex, *GSA Bull.,* **107**(12), 1468–1483.

Fletcher, R.C. & Hallet, B., 1983. Unstable extension of the lithosphere: a mechanical model for Basin-and-Range structure, *J. geophys. Res.,* **88**(B9), 7457–7466.

Friedl, N., Rammerstorfer, F.G. & Fischer, F.D., 2000. Buckling of stretched strips, *Comput. Struct.,* **78,** 185–190.

Gans, P.B., 1987. An open-system, two-layer crustal stretching model for the eastern Great Basin, *Tectonics,* **6,** 1–12.

Goetze, C. & Evans, B., 1979. Stress and temperature in the bending lithosphere as constrained by experimental rock mechanics, *Geophys. J. Int.,* **59,** 463–478.

Hammond, W.C. & Thatcher, W., 2004. Contemporary tectonic deformation of the Basin and Range province, western United States: 10 years of observation with the Global Positioning System, *J. geophys. Res.,* **109,** doi:10.1029/2003JB002746.

Hammond, W.C. & Thatcher, W., 2005. Northwest Basin and Range tectonic deformation observed with the Global Positioning System, 1999–2003, *J. geophys. Res.,* **110,** doi:10.1029/2005JB003678.

Janecke, S.U., Vanderburg, C.J. & Blankenau, J.J., 1998. Geometry, mechanisms and significance of extensional folds from examples in the Rocky Mountain Basin and Range province, U.S.A., *J. Struct. Geol.,* **20**(7), 841–856.

Jolivet, L., 2001. A comparison of geodetic and finite strain in the Aegean, geodynamic implications, *Earth. planet. Sci. Lett.,* **187,** 95–104.

Jolivet, L. & Faccenna, C., 2000. Mediterranean extension and the Africa-Eurasia collision, *Tectonics,* **19**(6), 1095–1106.

Jolivet, L., Famin, V., Mehl, C., Parra, T., Aubourg, C., Hébert, R. & Philippot, P., 2004. Strain localization during crustal-scale boudinage to form extensional metamorphic domes in the Aegean Sea, in *Gneiss Domes in Orogeny,* GSA Special Paper 380, pp. 185–210, eds Whitney, D.L., Teyssier, C. & Siddoway, C. S., Geol. Soc. Am., Boulder, CO.

Jongsma, D., 1974. Heat flow in the Aegean Sea, *Geophys. J. Int.,* **37,** 337–346.

Kaufman, P.S. & Royden, L.H., 1994. Lower crustal flow in an extensional setting: constaints from Halloran Hills region, eastern Mojave Desert, California, *J. geophys. Res.,* **99,** 15 723–15 739.

Kaus, B.J.P. & Schmalholz, S.M., 2006. 3D finite amplitude folding: implications for stress evolution during crustal and lithospheric deformation, *Geophys. Res. Lett.,* **33,** doi:10.1029/2006GL026341.

King, G. & Ellis, M., 1990. The origin of large local uplift in extensional regions, *Nature,* **348,** 689–693.

Klemperer, S.L., Hauge, T.A., Hauser, E., Oliver, J.E. & Potter, C.J., 1986. The Moho in the northern Basin and Range province, Nevada, along the COCORP 40°N seismic reflection transect, *GSA Bull.,* **97,** 603–618.

Kruse, S., McNutt, M., Phipps-Morgan, J. & Royden, L., 1991. Lithospheric extension near Lake Mead, Nevada—a model for ductile flow in the lower crust, *J. geophys. Res.,* **96,** 4435–4456.

Lachenbruch, A.H. & Sass, J.H., 1978. Models of an extending lithosphere and heat flow in the Basin and Range province, in *Cenozoic Tectonics and Regional Geophysics of the Western Cordillera,* GSA Memoir 152, pp. 209–250, eds Smith, R.B. & Eaton, G.P., Geol. Soc. Am., Boulder, CO.

Landau, L.D. & Lifshitz, E.M., 1986. *Theory of Elasticity, vol. 7 of Course of Theoretical Physics,* Pergamon Press, Oxford.

Lowry, A.R. & Smith, R.B., 1994. Flexural rigidity of the Basin and Range-Colorado Plateau-Rocky Mountain transition from coherence analysis of gravity and topography, *J. geophys. Res.,* **99,** 20 123–20 140.

Mancktelow, N. & Pavlis, T., 1994. Fold-fault relationships in low-angle detachment systems, *Tectonics,* **13**(2), 668–685.

Marques, F.O. & Podladchikov, Y.Y., 2009. A thin elastic core can control large-scale patterns of lithosphere shortening, *Earth planet. Sci. Lett.,* **277,** 80–85.

Martinod, J. & Davy, P., 1992. Periodic instabilities during compression or extension of the lithosphere 1. Deformation modes from an analytical perturbation method, *J. geophys. Res.,* **97,** 1999–2014.

McClusky, S. *et al*., 2000. Global Positioning System constraints on plate kinematics and dynamics in the eastern Mediterranean and Caucasus, *J. geophys. Res.,* **105,** 5695–5720.

McKenzie, D., Nimmo, F., Jackson, J.A., Gans, P.B. & Miller, E.L., 2000. Characteristics and consequences of flow in the lower crust, *J. geophys. Res.,* **105,** 11 029–11 046.

Parsons, T., Thompson, G.A. & Smith, R.P., 1998. More than one way to stretch: a tectonic model for extension along the plume track of the Yellowtsone hotspot and ajacent Basin and Range province, *Tectonics,* **17**(2), 221–234.

Ricard, Y. & Froidevaux, C., 1986. Stretching instabilities and lithospheric boudinage, *J. geophys. Res.,* **91,** 8314–8324.

Schlische, R.W., 1995. Geometry and origin of fault-related folds in extensional settings, *AAPG Bull.,* **79**(11), 1661–1678.

Schmalholz, S.M., 2008. 3D numerical modeling of forward folding and reverse unfolding of a viscous single-layer: implications for the formation of folds and fold patterns, *Tectonophysics,* **446,** 31–41.

Schmalholz, S.M., Podladchikov, Y.Y. & Jamtveit, B., 2005. Structural softening of the lithosphere, *Terra Nova,* **17**(1), 66–72.

Spencer, J.E. & Chase, C.G., 1989. Role of crustal flexure in initiation of low-angle normal faults and implications for structural evolution of the Basin and Range Province, *J. geophys. Res.,* **94,** 1765–1775.

Tirel, C., Gueydan, F., Tiberi, C. & Brun, J., 2004. Aegean crustal thickness inferred from gravity inversion. Geodynamical implications, *Earth planet. Sci. Lett.,* **228,** 267–280.

Turcotte, D.L. & Schubert, G., 1982. *Geodynamics, Applications of Continuum Physics to Geological Problems,* John Wiley and Sons, New York, NY.

Wijns, C., Weinberg, R., Gessner, K. & Moresi, L., 2005. Mode of crustal extension determined by rheological layering, *Earth planet. Sci. Lett.,* **236,** 120–134.

Yin, A., 1991. Mechanisms for the Formation of domal and basinal detachment faults: a three-dimensional analysis, *J. geophys. Res.,* **96,** 14 577–14 594.

Zoback, M.L. & Thompson, G.A., 1978. Basin and Range rifting in northern Nevada: clues from a mid-Miocene rift and its subsequent offsets, *Geology,* **6,** 111–116.

Zoback, M.L. & Zoback, M.D., 1989. Tectonic stress field of the continental U.S., in *Geophysical Framework of the Continental United States,* GSA Memoir 172, pp. 523–539, eds Pakiser, L. & Mooney, W., Geol. Soc. Am., Boulder, CO.

Zuber, M.T., Parmentier, E.M. & Fletcher, R.C., 1986. Extension of continental lithosphere—a model for two scales of basin and range deformation, *J. geophys. Res.,* **91,** 4826–4838.

APPENDIX A: FOLD CHARACTERISTICS FOR AN ISOLATED ELASTIC SHEET

The wavelength λ and amplitude A are obtained by minimizing the total energy U of the elastic sheet, and by taking into account an inextensibility condition in a direction perpendicular to stretching. The energy U can be written as

$$U = U_b + U_s, \tag{A1}$$

where U_b and U_s are the bending and stretching energies of the sheet, respectively.

In view of our experiments, we will assume that the shape ζ of the wrinkles is to the first-order well-described by sinusoidal functions

$$\zeta = A \sin\left(\frac{\pi x}{L}\right) \sin\left(\frac{2\pi y}{\lambda}\right). \tag{A2}$$

A1 Bending energy

The bending of the sheet induces compressive stresses in the inner part of the folds and extensive stresses in their outer part. For sufficiently small amounts of flexure, the neutral line between the extending and contracting domains is at mid-thickness of the sheet. We take this assumption for the following calculations. The stress σ and strain ε associated with the bending of a thin plate are in this case

$$\sigma = \frac{E}{1-\nu^2} z \frac{\partial^2 \zeta}{\partial y^2} \quad \text{and} \quad \varepsilon = z \frac{\partial^2 \zeta}{\partial y^2}, \tag{A3}$$

where ζ is the vertical displacement of a point of the plate caused by the bending (Landau & Lifshitz 1986). The bending energy is

$$U_b = \int_0^W \int_0^L \int_{-\frac{h}{2}}^{\frac{h}{2}} \sigma \varepsilon \, \mathrm{d}z \mathrm{d}x \mathrm{d}y, \tag{A4}$$

$$U_b = \frac{1}{2} \int_0^W \int_0^L D \left(\frac{\partial^2 \zeta}{\partial y^2}\right)^2 \mathrm{d}x \mathrm{d}y \quad \text{with} \quad D = \frac{E h^3}{12(1-\nu^2)}. \tag{A5}$$

Replacing ζ by its expression (eq. A2) leads to

$$U_b = 2 D A^2 \left(\frac{\pi}{\lambda}\right)^4 L W. \tag{A6}$$

A2 Stretching energy

The force applied in the longitudinal direction to stretch the sheet is

$$F = \int_0^W T \, \mathrm{d}y, \tag{A7}$$

with $T = E\gamma\, h$. It induces an extension

$$\mathrm{d}l = \sqrt{\mathrm{d}x^2 + \mathrm{d}\zeta^2} - \mathrm{d}x, \tag{A8}$$

which gives to the first order

$$\mathrm{d}l \sim \frac{1}{2} \left(\frac{\partial \zeta}{\partial x}\right)^2 \mathrm{d}x, \tag{A9}$$

assuming that the vertical displacement is small compared to $\mathrm{d}x$.

The stretching energy is therefore

$$U_s = \int_0^L F \mathrm{d}l, \tag{A10}$$

$$U_s = \frac{1}{2} \int_0^W \int_0^L T \left(\frac{\partial \zeta}{\partial x}\right)^2 \mathrm{d}x \mathrm{d}y. \tag{A11}$$

Using eq. (A2), we obtain

$$U_s = \frac{\pi^2}{8} T A^2 \frac{W}{L}. \tag{A12}$$

A3 Condition of inextensibility

Shortening in the Oy-direction is $\mathrm{d}w = \sqrt{\mathrm{d}y^2 + \mathrm{d}\zeta^2} - \mathrm{d}y$, which gives to the first order

$$\mathrm{d}w \sim \frac{1}{2} \left(\frac{\partial \zeta}{\partial y}\right)^2 \mathrm{d}y. \tag{A13}$$

We can write

$$\int_0^L \int_0^W \frac{1}{2} \left(\frac{\partial \zeta}{\partial y}\right)^2 \mathrm{d}y \mathrm{d}x = \int_0^L \int_0^W \frac{\Delta(x)}{W} \mathrm{d}y \mathrm{d}x, \tag{A14}$$

where $\Delta(x)$ is the shortening induced by the stretching.

With our expression of ζ (eq. A2), this leads to

$$A^2 W = \frac{2\lambda^2 \bar{\Delta}}{\pi^2}, \tag{A15}$$

where $\bar{\Delta}$ is the average transverse shortening.

A4 Expressions of A and λ

Combining eqs (A6), (A12) and (A15), we get

$$U = \bar{\Delta} \left(\frac{4\pi^2}{\lambda^2} D L + \frac{1}{4} T \frac{\lambda^2}{L}\right). \tag{A16}$$

The wavelength which minimizes U is

$$\lambda = 2\sqrt{\pi L} \left(\frac{B}{T}\right)^{1/4}. \tag{A17}$$

The corresponding amplitude is obtained from eq. (A15)

$$A = \frac{\lambda}{\pi} \left(2\frac{\bar{\Delta}}{W}\right)^{1/2}. \tag{A18}$$

If we assume that the average transverse shortening is $\bar{\Delta} = \nu\gamma W$, we finally get

$$A = (\nu L h)^{\frac{1}{2}} \left[\frac{16\gamma}{3\pi^2(1-\nu^2)}\right]^{\frac{1}{4}}, \tag{A19}$$

$$\lambda = \frac{(2\pi L h)^{\frac{1}{2}}}{\left[3(1-\nu^2)\gamma\right]^{\frac{1}{4}}}. \tag{A20}$$

APPENDIX B: ACCOUNTING FOR DEFORMATION BENEATH THE ELASTIC LAYER AND GRAVITY

B1 Variation of potential energy

We consider a crust of initial thickness h_i and density ρ_c. Stretched in the Ox-direction (Fig. 14), it folds and undergoes lateral shortening in the Oy-direction. The crustal thickness increases and becomes $h_f = h_i(1+\Delta)$, where Δ is the transverse shortening ($\Delta = \Delta W/W$,

see eq. 5). We assume that the surface folds are not compensated isostatically, because of their small wavelength, but the augmentation of the crustal thickness implies a large-scale compensation. We calculate the potential energy of the system for a constant mass, by length unit in the *Ox*-direction. The mass unit that we consider is $h_f\lambda$, which corresponds in the reference state to $h_i(1 + 2\nu\gamma)\lambda$. The potential energy in the initial and folded states are therefore

$$U_{ini} = \rho_c g \int_0^{\lambda(1+2\nu\gamma)} \int_{h_f-h_i-h_a}^{h_f-h_a} z \, dz \, dy \, , \tag{B1}$$

$$U_{fin} = \rho_c g \int_0^{\lambda} \int_0^{h_f+A\sin(ky)} z \, dz dy. \tag{B2}$$

The variation of potential energy obtained after integration is

$$\Delta U_{pot} = \rho_c g\lambda \frac{A^2}{4} + \rho_c g\lambda\nu\gamma h_i^2(1 + 2\nu\gamma)\left(1 - 2\frac{\rho_c}{\rho_m}\right). \tag{B3}$$

B2 Bending energy

We rewrite the stress and strain associated to the bending of a thin plate (eq. A3) with scaling lengths. We obtain

$$\sigma = E_s h \frac{A}{\lambda^2} \quad \text{and} \quad \varepsilon = \frac{hA}{\lambda^2}. \tag{B4}$$

The bending energy of the elastic surface layer is then

$$U_b = \sigma\varepsilon h\lambda = E_s h^3 \frac{A^2}{\lambda^3}. \tag{B5}$$

B3 Stretching energy

The stretching energy by length unit in the *Ox*-direction is obtained from eq. (A12):

$$U_s = \frac{1}{2}\int_0^W E_s\gamma h \left(\frac{\partial\zeta}{\partial x}\right)^2 dy, \tag{B6}$$

which can be expressed with scaling lengths as

$$U_s = E_s\gamma h \frac{A^2}{\lambda}. \tag{B7}$$

B4 Energetic dissipation for a viscous substrate

In the case of a viscous substrate, the energetic dissipation is

$$U_{visc} = \eta \frac{A}{\lambda\tau}, \tag{B8}$$

where η is the viscosity and τ the time lapse required to get a deformation $\varepsilon = A/\lambda$.

B5 Energetic cost of the deformation of an elastic substrate

In the case of an elastic substrate, the variation of energy induced by its deformation is calculated assuming that it is thick enough to be assimilated to a half-space. With the characteristic lengths of the problem, the stress can be written as

$$\sigma = E_b \frac{A}{\lambda}, \tag{B9}$$

and the energy variation for the substrate by length unit is

$$U_{substrate} = \sigma A\lambda = E_b A^2. \tag{B10}$$

B6 Condition of inextensibility

The width variation (in the *Oy*-direction) is

$$dw = \sqrt{dy^2 + d\zeta^2} - dy. \tag{B11}$$

We can therefore write

$$\frac{dw}{dy} = \sqrt{1 + \left(\frac{\partial\zeta}{\partial y}\right)^2} - 1, \tag{B12}$$

which, using scaling lengths, leads to

$$\Delta \sim \sqrt{1 + \frac{A^2}{\lambda^2}} - 1 \tag{B13}$$

with Δ, the lateral deformation (see eq. 5),

$$\Delta = \frac{2\nu\gamma}{1 + 2\nu\gamma}. \tag{B14}$$

$\frac{A}{\lambda} \ll 1$, implying that, to first order, $A \sim \lambda\sqrt{\Delta}$.